

A unified nonempirical strength model

Xing Feng

Yanshan University

Guangpeng Sun

Yanshan University

Sitong Zhang

Yanshan University

Bin Wen (✉ wenbin@ysu.edu.cn)

Yanshan University

Research Article

Keywords: Strength, dislocation, 2D displacement potential of dislocation slipping, CRSS

Posted Date: February 10th, 2022

DOI: <https://doi.org/10.21203/rs.3.rs-1340677/v1>

License:  This work is licensed under a Creative Commons Attribution 4.0 International License.

[Read Full License](#)

A unified nonempirical strength model

Xing Feng[†], Guangpeng Sun[†], Sitong Zhang, Bin Wen*

Center for High Pressure Science, State Key Laboratory of Metastable Materials Science and Technology, Yanshan University, Qinhuangdao 066004, China

Abstract Strength, as an important indicator of structural materials, has always been an important research topic in materials science. Theoretically, building a strength model is a rewarding method to understand the relationship between the mechanical properties and microstructure of materials. Although many strength models can reduplicate experimental values very well, they are empirical models, and their applicability is limited to materials for which empirical parameters have been obtained. Here, a nonempirical strength model is proposed based on the two-dimensional (2D) displacement potential of dislocation slipping, which can be applied to different chemically bonded crystals. Owing to the large electron localization function (ELF), covalent and ionic crystals have a high 2D displacement potential of dislocation slipping, and their dislocation slip mode prefers the kink-pair mode, further exhibiting a high critical resolved shear stress (CRSS). In contrast, metallic crystals with a small ELF have a low 2D displacement potential of dislocation slipping, and their dislocation slip mode is more inclined to the string mode, showing a low CRSS. This work provides new insights into dislocation-slipping configurations that will be useful for the development of new high-performance structural materials.

Keywords: Strength; dislocation; 2D displacement potential of dislocation slipping; CRSS

[†] These authors contributed equally to this work.

* Corresponding author, E-mail address: wenbin@ysu.edu.cn

1. Introduction

With the rapid development of science and technology, the service environment of structural materials has become increasingly harsh¹. To ensure the reliability and durability of engineering components, structural materials with very high performance are needed, and a very deep understanding of their strengthening mechanism is necessary. Since the strength is closely related to the microstructure, understanding and constructing the correlation between the strength and microstructure has always been an important research topic in materials science²⁻⁵.

As early as 1926, a theoretical strength model was proposed by Frenkel⁶. However, the strength calculated by this model is several orders of magnitude higher than the experimental observation. Therefore, this model is inadequate for calculating and understanding the strength of materials.

To date, according to the principle on which strength models are based, they have been categorized into two categories, which can be used to obtain strengths similar to experimental values. One category is based on dislocation theory, and these models are usually used to study the yield strength of metallic materials. The other category is based on valence bond theory, and these models are usually used to study the hardness of covalent and ionic materials.

For the yield strength models based on dislocation theory, the original model is the Peierls-Nabarro (P-N) model^{7,8}. In the P-N model, a one-dimensional (1D) displacement potential (P-N barrier) is used, and a nonempirical expression of the force required for dislocation motion (P-N force) is given. Although the predicted P-N force is consistent with the experimental results in terms of the order of magnitude, the temperature and strain rate effects on the strength cannot be considered in this model⁹. To overcome this drawback, two empirical models have been built on the basis of transmission electron microscopy (TEM) observations and the 1D P-N barrier. One is the

Seeger model (kink-pair model)^{10,11}, which is applicable to some covalent materials¹² or body-centred-cubic (BCC) metallic materials¹³. The other model is the string model, which was built by Friedel in 1959¹⁴ and is applicable to some metallic materials¹⁵. Although thermal activation for dislocation movement has been considered and the predicted strength is consistent with the experimental results^{11,13,16,17}, their application scope is questioned owing to the empirical dislocation slipping mode used. Hence, the use of these models in the design of mechanical properties for new materials is unreliable.

The strength (hardness) models based on valence bond theory are mainly for covalent and ionic materials¹⁸⁻²³. Currently, only the properties of chemical bonds are considered in all these models. According to these models, single-crystal diamond should obviously be the hardest material because the sp^3 hybridized C–C bond in diamond is the strongest bond in the three-dimensional network²⁴. However, recently synthesized nanotwinned diamond is more than twice as hard as single-crystal diamond²⁵. Obviously, explaining the hardening mechanism of covalent materials based only on these hardness models is unreasonable, and a more profound theory is urgently needed to investigate the hardness of covalent and ionic crystals.

Previous studies have proven that some metallic bonds are weakly directional, similar to covalent bonds²⁶. For covalent crystals, dislocation theory is utilized to understand the origin of the hardness of nanotwinned diamond^{12,27,28}. These cases offer a feasible means: a unified strength model based on dislocation theory can be used to deal with metallic, covalent, and ionic materials. The displacement potential of dislocation slipping has been found to be dominated by the two adjacent atomic planes in a crystal lattice, and the dislocation bends and kinks when moving on its slip plane²⁹; therefore, the displacement potential of dislocation slipping should be considered a

two-dimensional (2D) potential. Naturally, the joint influence of the directionality and strength of the chemical bonds on a dislocation can be included. Based on this idea, a unified strength (yield strength/hardness) model for different chemically bonded crystals is proposed in this work. This will provide insight into the physical mechanism of the dislocation slipping mode and strength, which will be helpful for designing and studying structural materials.

2. Origin of different dislocation slipping modes in the 2D displacement potential

A dislocation is a line defect on a slip plane, and its motion is limited to its slip plane. At finite temperatures, thermal activity is essential; hence, the dislocation slipping mode is dominated not only by mechanical activation but also by thermal activation. Therefore, a dislocation slipping by keeping a straight line mode (P-N model) with invalid thermal activation is infeasible, and an actual dislocation slipping mode should be partially protruding¹¹. In this situation, the displacement potential of dislocation slipping includes not only the 1D P-N barrier (E_{PN}) but also the migration barrier (E_M) of sideways movement of the protruding parts. These two barriers distribute in mutual angle directions and constitute a 2D barrier surface, which not only restricts the expansion of dislocation lines but also restricts the shape of dislocation motion and affects its slipping mode³⁰.

The 2D barrier obstructing dislocation motion is related to the crystal structure and dislocation properties^{7,8}, such as shear modulus G , Poisson's ratio ν , and Burgers vector b . Thus, the 2D barrier is an intrinsic property of a material. Under finite temperature T and applied shear stress τ conditions, both temperature and shear stress contribute to overcoming this 2D barrier, and the slipping mode varies with temperature and applied shear stress³¹. According to the relative energies of the thermal activation energy $mk_B T$ (k_B is the Boltzmann constant, and m is a coefficient³²) and

E_M as well as E_{PN} , the slipping mode can be divided into four categories (as shown in Fig. 1):

1. **Hard kink-pair mode** When the temperature is low, thermal activation cannot overcome barriers in any direction. At this time, all protruding dislocation segments are straight in three directions due to the restrictions from E_{ML} , E_{MR} , and E_{PN} , as shown in Fig. 1(a).

2. **Mixed kink-pair mode** When the thermal activation energy is higher than E_{ML} but lower than E_{MR} ($E_{ML} < mk_B T < E_{MR} < E_{PN}$), the thermal activation overcomes the left migration barrier. Accordingly, the left dislocation segment transforms into the string mode, which is bounded only by its line tension. However, the dislocation in such a temperature range is still constrained by E_{MR} and E_{PN} , and the other two dislocation segments are straight, as shown in Fig. 1(b).

3. **Soft kink-pair mode** When the thermal activation energy is higher than E_{ML} and E_{MR} but smaller than E_{PN} , *i.e.*, $E_{ML} < E_{MR} < mk_B T < E_{PN}$, the thermal activation overcomes the left and right migration barriers. Therefore, the left and right dislocation segments transform into the string mode, but the dislocation segment perpendicular to E_{PN} remains straight, as shown in Fig. 1(c).

4. **String mode** With increasing temperature, thermal activation overcomes barriers in any direction, and all protruding dislocation segments enter the string mode, which is only bounded by the line tension, as shown in Fig. 1(d).

3. Mathematical model of material strength

3.1 Critical resolved shear stress (CRSS) of dislocation slip

To obtain the CRSS of dislocation slip, the energy of the dislocation system is mathematically modelled for nucleation and expansion in different slipping modes. In this work, the energy of the dislocation system includes four parts: elastic energy, interaction energy, work done by the applied

shear stress, and stacking fault energy. Because the dislocation core energy is approximately 1/10~1/15 of the elastic energy⁹, it is ignored.

For the hard kink-pair mode, as shown in Fig. 1(a), the energy of the dislocation system can be expressed as a function of the applied shear stress τ and nucleus size x :

$$E(x, \tau) = \frac{A_1 G b^2 h}{2\pi} \ln\left(\frac{R_i}{r}\right) - \frac{A_2 G b^2 h^2}{8\pi x} - h b x \tau + h x \gamma_{SEF}, \quad (1)$$

where $A_1 = \cos^2 \beta + \frac{\sin^2 \beta}{1-\nu}$, $A_2 = \frac{(1+\nu) \cos^2 \beta + (1-2\nu) \sin^2 \beta}{1-\nu}$, β is the angle between the dislocation line and Burger's vector b , h is the kink height, R_i is the integral range of linear elasticity theory, r is the dislocation core radius, and γ_{SEF} is the stacking fault energy.

For the mixed kink-pair mode, as shown in Fig. 1(b), the energy of the dislocation system can also be expressed as a function of τ and x :

$$E(x, \tau) = \frac{sE_0}{\cos(\theta + \alpha)} + \frac{lE_0 \cos(\theta - \alpha)}{\cos(\theta + \alpha)} + \frac{A_1 G h b^2}{4\pi} \ln\left(\frac{R_i}{r}\right) - xE_0 - \frac{A_2 G b^2 h^2}{8\pi x} - \left[\frac{1}{2}(l+x)h + R^2 \left(\alpha - \frac{1}{2} \sin 2\alpha \right) \right] b\tau + \left[\frac{1}{2}(l+x)h + R^2 \left(\alpha - \frac{1}{2} \sin 2\alpha \right) \right] \gamma_{SEF}, \quad (2)$$

where s is the length of the arc (R is the radius), l is the length of the partial protrusion, 2α is the central angle of the arc, and $E_0 = \frac{1}{2} G b^2$ is the energy per unit length of the straight dislocation.

For the soft kink-pair mode, as shown in Fig. 1(c), the energy of the dislocation system can also be expressed as a function of τ and x :

$$E(x, \tau) = \frac{2sE_0}{\cos(\theta + \alpha)} + \frac{lE_0 \cos(\theta - \alpha)}{\cos(\theta + \alpha)} - xE_0 - \frac{A_2 G b^2 h^2}{8\pi x} - \left[\frac{1}{2}(l+x)h + 2R^2 \left(\alpha - \frac{1}{2} \sin 2\alpha \right) \right] b\tau + \left[\frac{1}{2}(l+x)h + 2R^2 \left(\alpha - \frac{1}{2} \sin 2\alpha \right) \right] \gamma_{SEF}. \quad (3)$$

For the string mode, as shown in Fig. 1(d), the energy of the dislocation system can be expressed as a function of τ and nucleus size R :

$$E(R, \tau) = 2R\beta \frac{E_0}{\cos \beta} - 2R \sin \beta E_0 - b\tau R^2 \left(\beta - \frac{1}{2} \sin 2\beta \right) + R^2 \left(\beta - \frac{1}{2} \sin 2\beta \right) \gamma_{SEF}, \quad (4)$$

where 2β is the central angle of the string.

When τ is given, the energy of the dislocation system, E , is a function of the nucleus size x or R . As schematically shown in Fig. 2(a), the energy of the dislocation system initially increases, followed by a decrease as the nucleus size keeps increasing. There exists a maximum of the energy, which is called the thermal activation energy barrier $Q(\tau)$ for dislocation motion at a given applied shear stress τ . Mathematically, $Q(\tau)$ can be determined by calculating the first derivative of E with respect to x or R . Therefore, $Q(\tau)$ as a function of τ can be obtained, as schematically shown in Fig. 2(b). For all four slipping modes, $Q(\tau)$ monotonically decreases with increasing τ . Under the same applied shear stress, the dislocation slipping mode with a low activation energy barrier is priority activated. E_{PN} , E_{ML} , and E_{MR} equivalently decrease with increasing τ . The final dislocation slipping mode is determined by two factors: one is the relative energies of the thermal activation energy $mk_B T$ and E_M as well as E_{PN} , as mentioned in Section 2, and the second factor is the competition between different slipping modes to ensure a lower energy barrier.

By combining the Orowan equation³³⁻³⁵ and Arrhenius's dislocation velocity expressions³⁶, the following relationship can be obtained:

$$Q(\tau) = k_B T \ln \left(\frac{\rho_m b \lambda \nu_D}{\dot{\epsilon}} \right), \quad (5)$$

where ρ_m is the density of movable dislocations; λ_b is the average free path of dislocations; ν_D is the Debye frequency of the material; and $\dot{\epsilon}$ is the strain rate.

By solving Eq. 5, the CRSS can be obtained for given temperature, dislocation density, and strain rate.

3.2 Nonempirical strength model for polycrystalline materials

A polycrystalline material is composed of many single-crystal grains with different orientations, and a single crystal grain with high symmetry, such as face-centred-cubic (FCC) and BCC crystals, exhibits a multiple slip system. Although the CRSS can characterize the critical shear strength of dislocation motion on a single slip plane and dominate the strength of a polycrystalline material, the CRSS cannot be directly used as the strength of a polycrystalline material, and there exists a geometric transformation between them. Usually, the yield strength of polycrystalline materials can be calculated from the CRSS by using the Sachs model³⁷, the Taylor model³⁸, and the self-consistent (SC) model³⁹. In this work, the yield strength of polycrystalline materials is calculated from the CRSS by using the Sachs model as an example.

According to Schmid's law, the uniaxial yield stress of a single crystal is equal to the CRSS divided by the corresponding Schmid factor. Fig. 3(a) shows the distribution of the Schmid factor of a single slip system for an FCC crystal. For a high symmetry single crystal, e.g., an FCC crystal, there are multiple slip systems and 48 patches of the Schmid factor, and the distribution is shown in Figs. 3(b) and 3(c). However, the uniaxial yield stress of a single crystal can also be calculated by Schmid's law, as shown in Fig. 3(d). In polycrystalline materials, there are many single-crystal grains with different orientations, as shown in Fig. 3(e). Under the action of uniaxial stress, grains with different orientations have different yield stresses. With increasing uniaxial stress, the number of yielded grains increases. When the number of yielded grains reaches a specific proportion (e.g., 90%), the corresponding uniaxial stress is treated as the yield strength of the polycrystalline material by using the Sachs model, as shown in Fig. 3(f). Furthermore, the Vickers hardness of polycrystalline materials can be calculated by using Tabor's law⁴⁰; that is, the Vickers hardness is

approximately 2.74 times the yield strength of the polycrystalline material.

In Section 3.1, the CRSS of dislocation slip was calculated by using Eqs. 1-5. The physical meaning of all parameters used in Eqs. 1-5 is clear, and no empirical parameters are used in these equations. Furthermore, the yield strength and Vickers hardness for a polycrystalline material are completely dependent on the CRSS and orientations of different grains. Therefore, our strength model for polycrystalline materials is totally nonempirical, and its application scope is not constrained by sources of empirical parameters.

4. Universality and reliability of the strength model

To verify the universality and reliability of our nonempirical strength model, the strengths (yield strength/hardness) of six multicrystals with different chemical bond types (i.e., diamond and cubic BN with covalent bonds, NaCl and MgO with ionic bonds, and Cu and Al with metallic bonds) are calculated. Here, the material properties and dislocation type parameters used in the strength model are obtained by the first-principles method, which is described in Supplementary Discussions I and II. The calculated material property parameters, generalized stacking fault energy (GSFE) surface, and dislocation types are listed and plotted in Supplementary Tables 1, Figs. S1~S3, and Table 2, respectively.

By using the method described in Section 3, the strengths for the abovementioned six multicrystals are calculated, and they are plotted in Fig. 4 and Supplementary Fig. S4. All calculated strengths agree well with the experimental observations spanning a certain range of temperatures and strain rates⁴¹⁻⁴⁶, which implies the universality and reliability of our nonempirical strength model. For covalent crystals and ionic crystals, their Vickers hardness continuously decreases with

increasing temperature under a given dislocation density. There exist two distinct regimes with different temperature-softening rates, which is consistent with our previous result from the kink-pair model²⁷, and the reason is that the dominant dislocation type changes with increasing temperature. For metallic crystals Cu and Al, there also exist two distinct regimes with different temperature-softening rates, but this change is contributed by the change in the dislocation mode from the hard kink-pair mode to the string mode with increasing temperature. Recently, Lunev's molecular dynamic simulation results for UO₂⁴⁷ indicated that its dislocation slipping mode changes with applied shear stress and temperature. This consistency shows the rationality of our model to some extent.

For all studied crystals, one can note that the strength increases with increasing strain rate (Fig. 4 and Supplementary Fig. S4), which indicates a strain rate hardening behaviour⁴⁸. In addition, their strength increases with decreasing dislocation density due to the work-hardening mechanism that can be ignored under low dislocation density.

In addition, the activated dislocation types under various temperatures are counted (Supplementary Figs. S7~S10). The types of activated slip systems of the six multocrystal materials agree with experimental observations^{9,12,27,49,50}. This further confirms the universality of our nonempirical strength model, which can be adopted not only for covalent crystal research but also for ionic and metallic crystals. Moreover, it can duplicate experimental values very well, showing its reliability.

5. Reconciling chemical bonds and dislocations in the unified strength model

For a crystal material, its strength is directly related to its plastic deformation⁵¹ and is related to

its dislocation motion. From a microscopic point of view, dislocation motion is a chemical bond breaking and rebonding process; therefore, bond properties have an important effect on dislocation motion. For the strength model based on dislocation theory⁵², only dislocation defects are considered, and no bond properties are considered; therefore, this model can only be adopted for some metallic materials with less electron localization. For the hardness model based of valence bond theory¹⁸⁻²³, only bond properties are considered, and no dislocation defects are considered; therefore, this model can only be adopted for some covalent materials with high electron localization. The effect factor on strength is not fully considered in the previous two types of strength models. Even though some empirical parameters are used in these models, they can duplicate experimental values very well. However, this leads to these models being empirical, and their applicability is limited to the materials for which they were obtained.

The motion of dislocations is controlled by the combination of mechanical and thermal action (as schematically shown in Fig. 5a)³⁰. Mechanical action leads to a change in crystal cell shape and further affects bond properties. This leads to the energy for chemical bond breaking being lower (Fig. 5b). In our model, with increasing applied shear stress, the 2D displacement potential (including the P-N barrier and the migration barrier) monotonically decreases (in Fig. 2b), which is the result of mechanical action. A previous study revealed that the barrier for chemical bond breaking is quantitatively correlated with the difference in the degree of electron localization⁵³. To quantitatively discuss the effect of mechanical action on the 2D displacement potential, the electron localization function (ELF)⁵⁴ for crystals under shear conditions is calculated, and the results are shown in Supplementary Fig. S11. Under the same strain conditions, the difference in the ELF (Δ ELF) for covalent or ionic crystals is usually larger than that for metallic crystals. This means that there are

higher energy barriers for covalent or ionic crystal deformation than for metallic crystal deformation. The calculated ΔE_{LF} between a perfect bond and dislocation core (Supplementary Figs. S12~S13) also illustrates this point.

With increasing applied shear stress, the system energy increases through mechanical action, and the thermal activation barrier decreases (in Fig. 5c). Furthermore, the total energy barrier can be overcome by both mechanical and thermal actions. As schematically shown in Fig. 5(d), because thermal activation energy ΔG is proportional to temperature, at given movable dislocation density and strain rate, ΔG linearly increases with temperature. Therefore, the thermal activation energy ΔG is permanent for any crystal. For covalent and ionic crystals with high 2D displacement potential, a high mechanical action is needed to overcome the barrier of dislocation slipping, which leads to a high strength for these crystals. For metallic crystals with low 2D displacement potential, thermal activation has an important contribution to overcoming the barrier of dislocation slipping, which leads to a low strength for these crystals and a high temperature-softening rate.

Another function of mechanical action is to decrease the energy of the dislocation system by the work done by the applied shear stress. Therefore, the larger the activation volume is, the larger the effect of mechanical action. For different dislocation slipping modes, the activation volume is different, and the slope of energy with respect to the applied shear stress can directly reflect the activation volume (in Fig. 2b). For the string mode, line tension shortens the length of the dislocation line as much as possible, and the activation volume is larger than that of the hard kink-pair mode. The energy of the dislocation system is sensitive to the applied shear stress, and the slope of the energy with respect to the applied shear stress is larger than that for the hard kink-pair mode. This is a partial reason why the strength of a crystal with the string mode is usually lower

than that with the hard kink-pair mode.

In our model, the bond property effect on dislocation motion has been considered by establishing a 2D displacement potential of dislocation slipping, and this is the root of the universality of our nonempirical strength model. The reconciling of chemical bonds and dislocations makes our strength model applicable to different chemically bonded crystals.

6. Conclusions

By establishing a 2D displacement potential of dislocation slipping, a unified nonempirical strength model is proposed. In this strength model, both chemical bond and dislocation effects on strength can be considered, and it can be used to predict the strength of different chemically bonded crystals. For covalent crystals and ionic crystals that have large electron localization, the dislocation prefers to slip in the kink-pair mode, exhibiting high CRSS and high strength. In contrast, metallic crystals with low electron localization prefer the string mode since the 2D displacement potential can be easily overcome by thermal activation; thus, metallic materials usually have low CRSS and low strength. All parameters used in our model are meaningful and nonempirical, and its application scope is unlimited; hence, our model is helpful for revealing the physical mechanism of strength and provides a direct tool for the design of new structural materials.

Acknowledgement

This work was supported by the National Natural Science Foundation of China (Grant Nos. 51925105 and 51771165) and the National Key R&D Program of China (YS2018YFA070119).

Author contributions

B.W conceived the project. X.F., G.P.S. and S.T.Z performed the calculations. B.W., X.F., and G.P.S. analyzed the data and co-wrote the paper. All authors discussed the results and commented on the manuscript.

Competing interests

The authors declare no competing interests.

Data availability

The authors declare that the data supporting the findings of this study are available within the paper and its Supplementary Information files.

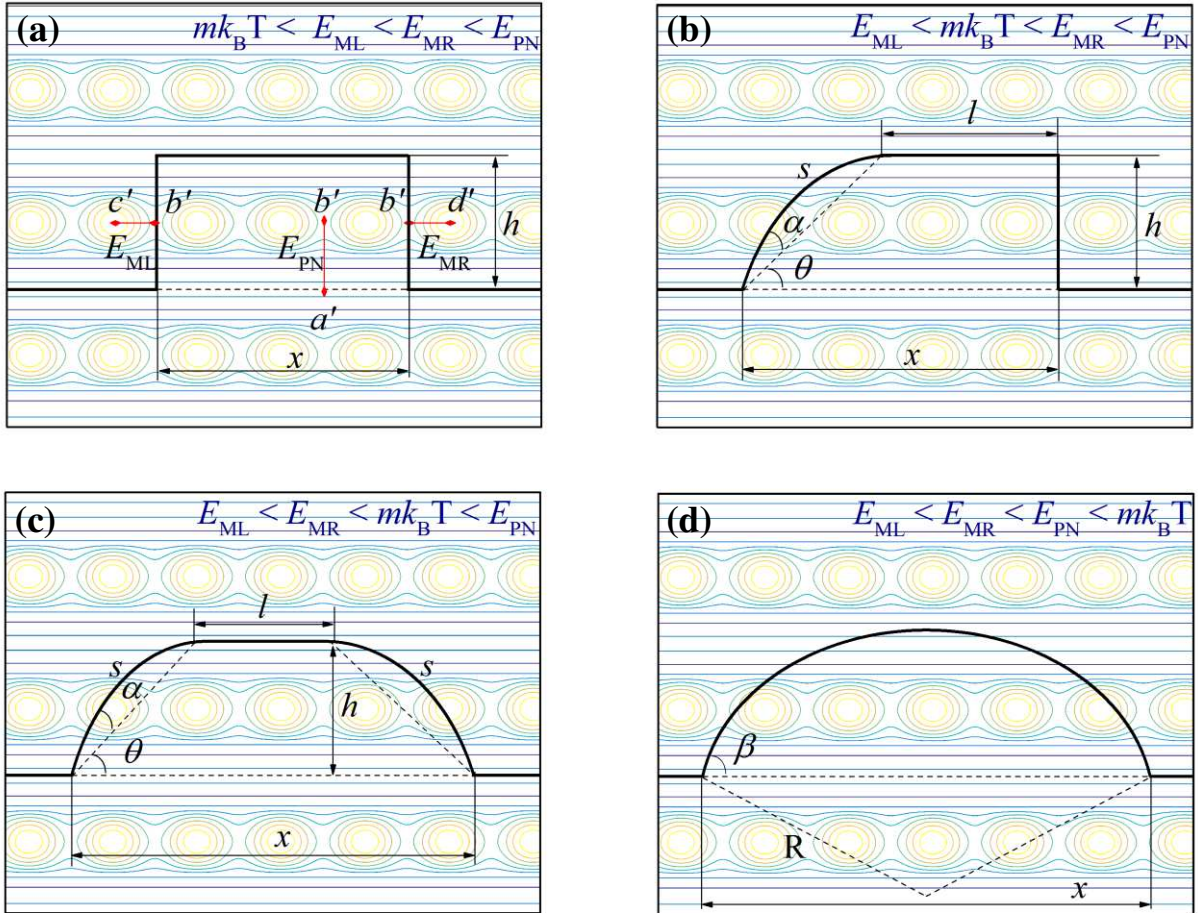


Fig. 1 2D displacement potential of dislocation slipping and origin of dislocation slipping modes. (a) Hard kink-pair mode. The black line represents the dislocation line configuration, and the background represents the projection of the 2D displacement potential, where the energy difference from the Peierls valley (a') to the saddle point (b') represents the P-N barrier (E_{PN}); the energy difference from the saddle point (b') to the left barrier peak (c') represents the left migration barrier (E_{ML}); and the energy difference from the saddle point (b') to the right barrier peak (d') represents the right migration barrier (E_{MR}). Furthermore, according to the restrictions from the 2D displacement potential on the dislocation, the dislocation slipping modes can be divided into mixed kink-pair mode (b), soft kink-pair mode (c), and string mode (d).

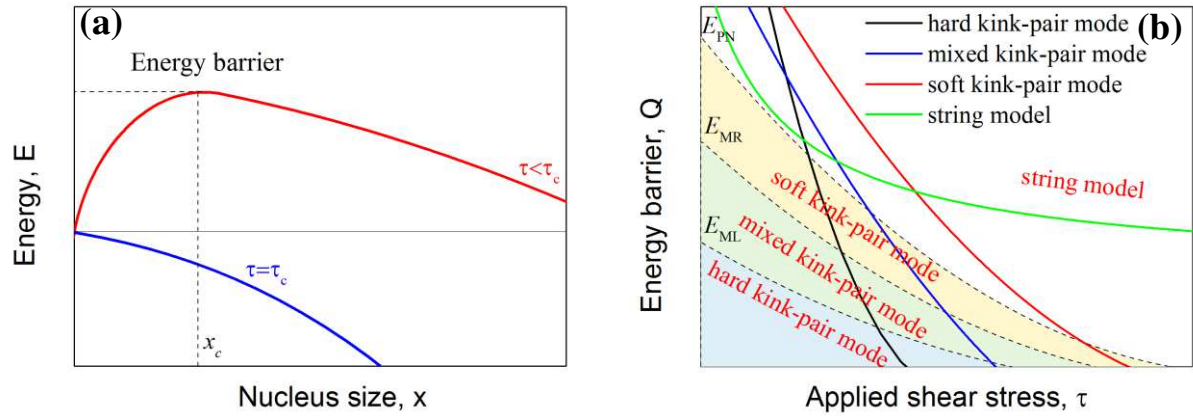


Fig. 2 Competition of dislocation slipping modes under a given applied shear stress. (a)

Dislocation system energy as a function of nucleus size under certainly applied shear stress. When the first derivative of the system energy reaches zero, the maximum value of the system energy can be defined as the thermal activation energy barrier, and x_c can be called the critical nucleus size. (b) Thermal activation energy barrier of the four dislocation slip modes as well as the E_{ML} , E_{MR} , and E_{PN} energy barriers.

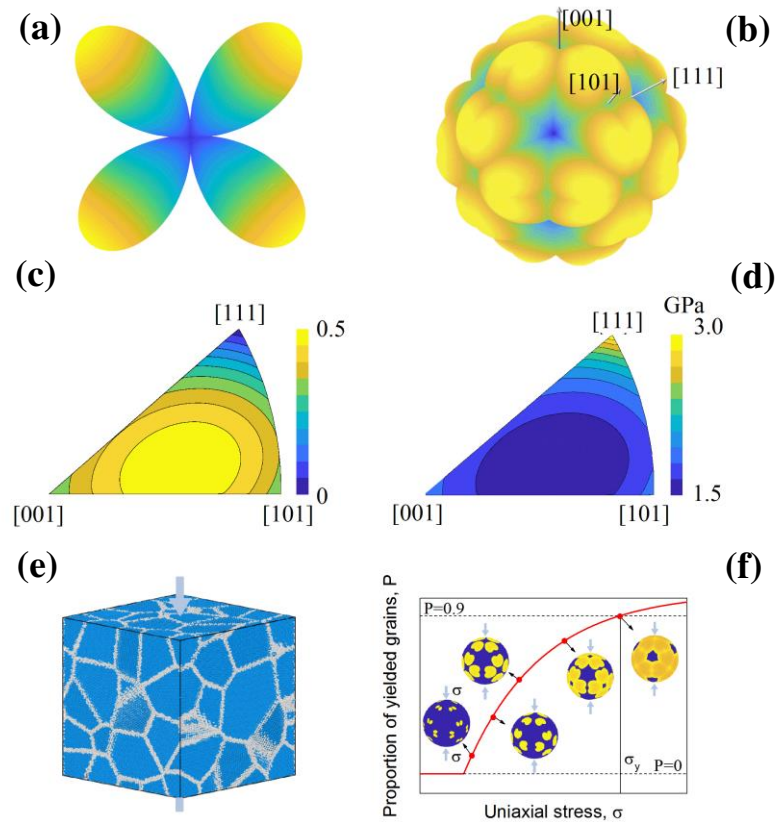


Fig. 3 Polycrystalline material strength calculation from the CRSS. (a) Three-dimensional plot of the Schmid factor distribution for a single slip system under different external force orientations. (b) Outer envelope of Schmid factors for 12 slip systems under different external force orientations. The grooves coincide with the edges of the characteristic triangle, where two slip systems are equally favoured. (c) Schmid factor of grains with different orientations under uniaxial stress conditions. (d) Yield strength of grains with different orientations. (e) Polycrystalline structure. (f) Population of yielded grains as a function of uniaxial stress.

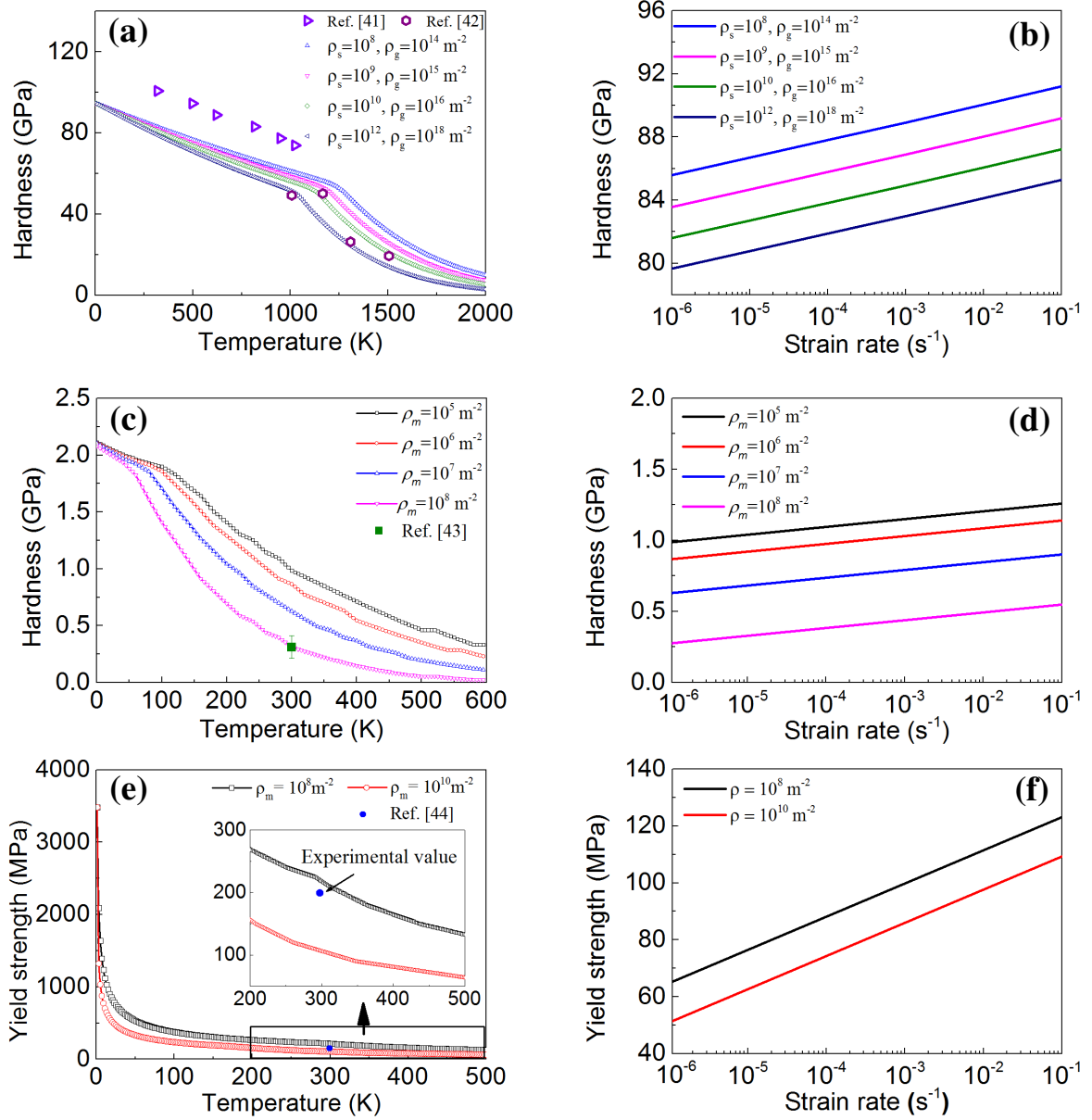


Fig. 4 Universality and reliability of our strength model. (a)-(b) The hardness of diamond varies as a function of temperature and strain rate. (c)-(d) The hardness of NaCl varies as a function of temperature and strain rate. (e)-(f) The yield strength of Cu varies as a function of temperature and strain rate.

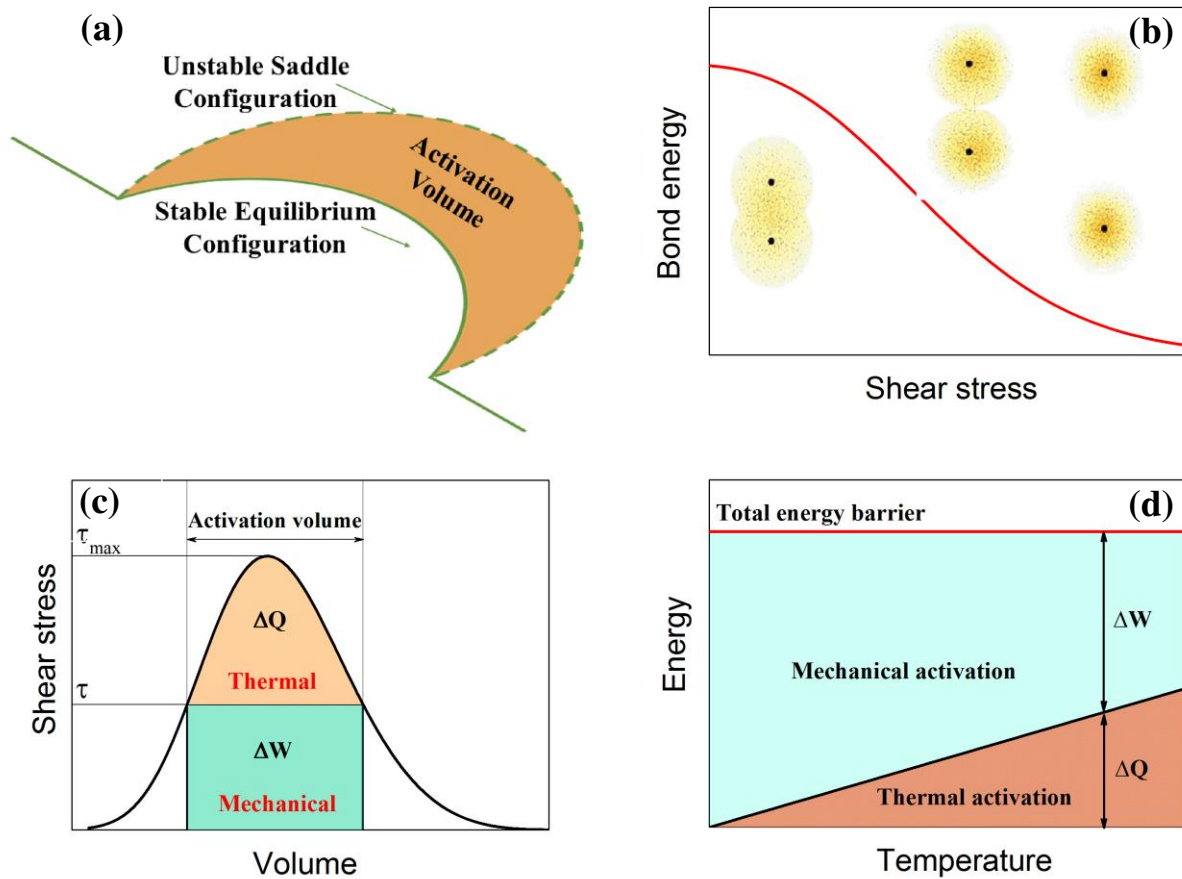


Fig. 5 Reconciling of chemical bonds and dislocations. (a) Schematic illustrating that the motion of a dislocation is controlled by the combination of mechanical and thermal actions. (b) Mechanical action leads to the energy for chemical bond breaking being lower. (c) Relationship between the mechanical and thermal activations. (d) Temperature-dependent mechanical and thermal activations.

References

- 1 Williams, J. C. & Starke Jr, E. A. Progress in structural materials for aerospace systems. *Acta Mater.* **51**, 5775-5799 (2003).
- 2 Wen, B. *et al.* Continuous strengthening in nanotwinned diamond. *npj Comput. Mater* **5**, doi:10.1038/s41524-019-0256-2 (2019).
- 3 Xiao, J. *et al.* Intersectional nanotwinned diamond-the hardest polycrystalline diamond by design. *npj Comput. Mater* **6**, 1-7 (2020).
- 4 Caillard, D. *Dislocations and mechanical properties.* (John Wiley & Sons Ltd, 2007).
- 5 Sun, G., Feng, X., Wu, X., Zhang, S. & Wen, B. Is hardness constant in covalent materials? *J. Mater. Sci. Technol.* **114**, 215-221, doi:10.1016/j.jmst.2021.10.032 (2022).
- 6 Frenkel, J. Zur theorie der elastizitätsgrenze und der festigkeit kristallinischer körper. *Z. Physik* **37**, 572-609 (1926).
- 7 Peierls, R. The size of a dislocation. *Proc. Phys. Soc.* **52**, 34 (1940).
- 8 Nabarro, F. Dislocations in a simple cubic lattice. *Proc. Phys. Soc.* **59**, 256 (1947).
- 9 Hull, D. & Bacon, D. J. *Introduction to dislocations.* (Butterworth-Heinemann, 2001).
- 10 Seeger, A. CXXXII. The generation of lattice defects by moving dislocations, and its application to the temperature dependence of the flow-stress of FCC crystals. *Philos. Mag.* **46**, 1194-1217 (1955).
- 11 Seeger, A., Donth, H. & Pfaff, F. The mechanism of low temperature mechanical relaxation in deformed crystals. *Discuss. Faraday Soc.* **23**, 19-30 (1957).
- 12 Xiao, J., Yang, H., Wu, X., Younus, F. & Tian, Y. Dislocation behaviors in nanotwinned diamond. *Sci. Adv.* **4**, eaat8195 (2018).
- 13 Seeger, A. & Wüthrich, C. Dislocation relaxation processes in body-centred cubic metals. *II Nuovo Cimento B* **33**, 38-75 (1976).
- 14 Freudenthal & A., M. Internal Stresses and Fatigue in Metals. *Phys. Today* **12**, 16-19 (1959).
- 15 Oh, S. H., Legros, M., Kiener, D. & Dehm, G. In situ observation of dislocation nucleation and escape in a submicrometre aluminium single crystal. *Nat. Mater.* **8**, 95-100 (2009).
- 16 Haasen, P. Plastic deformation of nickel single crystals at low temperatures. *Philos. Mag.* **3**, 384-418 (1958).
- 17 Conrad, H. Thermally activated deformation of metals. *Jom* **16**, 582-588 (1964).
- 18 Gao, F. *et al.* Hardness of covalent crystals. *Phys. Rev. Lett.* **91**, 015502 (2003).
- 19 Šimůnek, A. & Vackář, J. Hardness of covalent and ionic crystals: first-principle calculations. *Phys. Rev. Lett.* **96**, 085501 (2006).
- 20 Li, K., Wang, X., Zhang, F. & Xue, D. Electronegativity identification of novel superhard materials. *Phys. Rev. Lett.* **100**, 235504 (2008).
- 21 Lyakhov, A. O. & Oganov, A. R. Evolutionary search for superhard materials: Methodology and applications to forms of carbon and TiO₂. *Phys. Rev. B* **84**, 092103, doi:10.1103/PhysRevB.84.092103 (2011).
- 22 Mazhnik, E. & Oganov, A. R. A model of hardness and fracture toughness of solids. *J. Appl. Phys.* **126**, 125109 (2019).
- 23 Mazhnik, E. & Oganov, A. R. Application of machine learning methods for predicting new superhard materials. *J. Appl. Phys.* **128**, 075102, doi:10.1063/5.0012055 (2020).
- 24 Chaudhri, M. M. & Lim, Y. Y. Harder than diamond? Just fiction. *Nat. Mater.* **4**, 4 (2005).

- 25 Huang, Q. *et al.* Nanotwinned diamond with unprecedented hardness and stability. *Nature* **510**, 250-253 (2014).
- 26 Ogata, S., Li, J. & Yip, S. Ideal Pure Shear Strength of Aluminum and Copper. *Science* **298** (2002).
- 27 Feng, X. *et al.* Temperature-dependent hardness of zinc-blende structured covalent materials. *Sci. China Mater.* **16**, 2280–2288 doi:10.1007/s40843-020-1620-4 (2021).
- 28 Nie, A. *et al.* Direct observation of room-temperature dislocation plasticity in diamond. *Matter* **2**, 1222-1232 (2020).
- 29 JP, H., J, L. & T, M. Theory of Dislocations (2nd ed.). *J. Appl. Mech.* **50**, 476 (1983).
- 30 Caillard, D. & Martin, J.-L. *Thermally activated mechanisms in crystal plasticity*. (Elsevier, 2003).
- 31 Long, F., Xu, F. & Daymond, M. R. Temperature Dependence of the Activity of Deformation Modes in an HCP Zirconium Alloy. *Metall. Mater. Trans. A* **44**, 4183-4193, doi:10.1007/s11661-013-1758-z (2013).
- 32 George, A. & Rabier, J. Dislocations and plasticity in semiconductors. I—Dislocation structures and dynamics. *Rev. Phys. Appl.* **22**, 941-966 (1987).
- 33 Orowan, E. Plasticity of crystals. *Z. Phys* **89**, 605-659 (1934).
- 34 Schoeck, G. The activation energy of dislocation movement. *Phys. Status Solidi B* **8**, 499-507 (1965).
- 35 Hirth, J. & Nix, W. An analysis of the thermodynamics of dislocation glide. *Phys. Status Solidi B* **35**, 177-188 (1969).
- 36 Laidler, K. J. The development of the Arrhenius equation. *J. Chem. Educ.* **61**, 494 (1984).
- 37 Barnett, M. R., Keshavarz, Z. & X. Ma. A semianalytical Sachs model for the flow stress of a magnesium alloy. *Metall. Mater. Trans. A* **37A**, 2283-2293 (2006).
- 38 Taylor, G. I. Plastic strain in metals. *J. Inst. Metals* **62**, 307-324 (1938).
- 39 Hutchinson, J. Elastic-plastic behaviour of polycrystalline metals and composites. *Proc. R. Soc. London, Ser. A* **319**, 247-272 (1970).
- 40 Tabor, D. *The hardness of metals*. 553 (Oxford university press, 2000).
- 41 Weidner, D. J., Wang, Y. & Vaughan, M. T. Strength of diamond. *Science* **266**, 419-422 (1994).
- 42 Novikov, N. V., Sirota, Y. V., Mal'nev, V. I. & Petrusha, I. A. Mechanical properties of diamond and cubic BN at different temperatures and deformation rates *Diamond Relat. Mater.* **2**, 1253-1256 (1993).
- 43 Martienssen, W. & Warlimont, H. *Springer handbook of condensed matter and materials data*. (Springer Science & Business Media, 2006).
- 44 Li, M. & Zinkle, S. J. Physical and mechanical properties of copper and copper alloys. *Compr. Nucl. Mater.* **4**, 667-690 (2012).
- 45 Cáceres, D., Vergara, I., González, R. & Chen, Y. Hardness and elastic modulus from nanoindentations in nominally pure and doped MgO single crystals. *Philos. Mag. A* **82**, 1159-1171, doi:10.1080/01418610208240022 (2002).
- 46 Davis, J. R. *Aluminum and aluminum alloys*. 152-156 (ASM international, 1993).
- 47 Lunev, A., Starikov, S., Aliev, T. & Tseplyaev, V. Understanding thermally-activated glide of $1/2\langle 110 \rangle\{110\}$ screw dislocations in UO₂—a molecular dynamics analysis. *Int. J. Plast.* **110**, 294-305 (2018).

- 48 Ayres, R. A. & Wenner, M. L. Strain and strain-rate hardening effects in punch stretching of 5182-0 aluminum at elevated temperatures. *Metall. Trans. A* **10**, 41-46 (1979).
- 49 Riviere, A., Amirault, J. & Woirgard, J. High temperature internal friction and dislocation motion in poly and single crystals of fcc metals. *J. Phys. Colloques* **42**, 439-444 (1981).
- 50 Jo, M. *et al.* Theory for plasticity of face-centered cubic metals. *P Natl Acad Sci USA* **111**, 6560-6565 (2014).
- 51 Haines, J., Leger, J. & Bocquillon, G. Synthesis and design of superhard materials. *Annu. Rev. Mater. Res.* **31**, 1-23 (2001).
- 52 Hirth, J. A brief history of dislocation theory. *Metall. Mater. Trans. A* **16**, 2085-2090 (1985).
- 53 Zhang, Y. H., Zhuang, Y., Hu, A., Kai, J. J. & Liu, C. T. The origin of negative stacking fault energies and nano-twin formation in face-centered cubic high entropy alloys. *Scr. Mater.* **130**, 96-99, doi:10.1016/j.scriptamat.2016.11.014 (2017).
- 54 Becke, A. D. & Edgecombe, K. E. A simple measure of electron localization in atomic and molecular systems. *J. Phys. Chem.* **92**, 5397-5403, doi:10.1063/1.458517 (1990).

Supplementary Files

This is a list of supplementary files associated with this preprint. Click to download.

- [40250supp98074r6zfrg.pdf](#)